Binding-Induced Bond Polarization in Polymer Solutions to Drive Micelle and Vesicle Formation

Shubhra Goel,[1] Zitan Huang,[1] Robert A. Riggleman,[2] Ralph H. Colby,[1,3] and Robert J. Hickey[1,3,*]

[1]Department of Materials Science and Engineering, The Pennsylvania State University, University Park, Pennsylvania 16802, United States

[2]Department of Chemical and Biomolecular Engineering, University of Pennsylvania, Philadelphia, Pennsylvania 19104, United States

[3]Materials Research Institute, The Pennsylvania State University, University Park, Pennsylvania 16802, United States

*Corresponding Author Email: rjh64@psu.edu

For Table of Contents use only

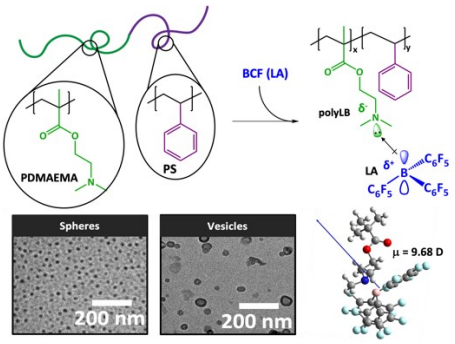

Abstract

Driving self-assembly through non-covalent interactions to create nanostructured materials is a key feature of supramolecular chemistry, yet the connection between molecular-level changes and larger-scale organization is still unknown. Here, we propose the concept of Lewis adduct binding-induced bond polarization where the formation of the Lewis adduct leads to a large

dipole, significantly altering the intermolecular interactions between different species and inducing self-assembly. Specifically, a diblock copolymer, poly(2-(dimethylamino)ethyl methacrylate)-polystyrene (PDMAEMA-PS), self-assembles into nanostructured colloidal aggregates on addition of the Lewis acid tris(pentafluorophenyl) borane (BCF) in toluene. The morphology of the nanostructured colloidal structures is controlled by tuning the block mole fraction of the poly(Lewis base) (polyLB, i.e., PDMAEMA) within the diblock copolymer, resulting in spherical micelles, vesicles, and large compound vesicles with increasing PDMAEMA block mole fraction. The self-assembly is driven by non-covalent binding-induced bond polarization during Lewis adduct formation, where the degree of bond polarization of the Lewis adducts were quantified by measuring the dielectric constant of adduct mixtures. We propose that the dipole formed because of the Lewis adduct leads to substantial changes in the polymer solvent interactions, driving the self-assembly. The reported findings regarding the Lewis adduct-induced self-assembly in polymer systems have far ranging potential implications in all non-covalent, intermolecular interactions that result in binding-induced bond polarization.

Keywords: Lewis Adducts, Block Copolymers, Self-Assembly, Micelles, Vesicles, Dielectric Constant

1. Introduction

Supramolecular materials formed by the dynamic non-covalent interactions are gaining tremendous attraction in self-assembled macromolecules due to responsive and self-healing properties.[1–4] The reversible nature of these non-covalent interactions provides a versatile mechanism for molecular self-assembly, facilitating the creation of a diverse array of well-defined nanostructures.[4–8] Non-covalent interactions include strong H-bonding, which stabilizes molecular structures through dipole-dipole attraction between an electronegative atom and a partially positive H-atom;[9–11] π-π stacking, essential for the organized assembly of aromatic compounds;[12–14] hydrophobic interactions, which drive the aggregation of non-polar molecules in aqueous environments;[15,16] ionic interactions, contributing electrostatic forces towards the assembly process;[16,17] metal-ligand coordination, which introduces metal centers into organic frameworks;[18,19] and one more such functionality that has garnered immense attention in research is Lewis adduct formation, where specific donor-acceptor interactions guide the assembly process.[20–23] Lewis acid chemistry is ideal for understanding how the strength of non-covalent bonding in supramolecular systems influence the self-assembly process and resulting nanostructures because the strength of the Lewis adduct, modulated by sterics and donor/acceptor electronics, is highly tunable. Although non-covalent, intermolecular interactions are broadly used for creating nanostructured colloids, materials, and gels, but the link between self-assembled structures and molecular changes through non-covalent interactions is still an open question.

Recently, the formation of Lewis adducts in polymer systems was found to induce a phase change at both the macroscopic and nanoscale levels. In this example, a post-polymerization modification approach demonstrated that the non-covalent dative bond formation by Lewis adducts using a poly(Lewis base) (polyLB) and a small molecule Lewis acid (LA) led to the phase change. Specifically, nanoscale spherical micelles formed when the

diblock copolymer poly(4-diphenylphosphinostyrene)-polystyrene (PDPPS-PS), where the PDPPS block acted as the polyLB and the PS block as a neutral component, was mixed with tris(pentafluorophenyl) borane (BCF), the LA. PDPPS-PS and LA are both independently soluble in toluene, but when mixed together, micellization occurs.[24,25] The proposed Lewis adduct induced self-assembly mechanism was attributed to the fact that the PDPPS/LA display an attractive interaction (i.e., quantified as a negative Flory-Huggins χ parameter), resulting in a demixing process for the ternary blend (i.e., polyLB, LA, and solvent). Although a three-component polymer solution mixing theory supported the results, the quantity of the Flory-Huggins χ parameter necessary to induce the phase change was exceptionally negative.[25] Therefore, the non-covalent, Lewis adduct bond is expected to play a significant role in changing the molecular environment that then leads to self-assembly.

Here, we reveal that the formation of a Lewis adduct leads to a bond polarization event that results in a significantly large dipole moment (i.e., 12.5 D) measured experimentally and supported through density functional theory (DFT) calculations. Thus, the dipole produced via non-covalent, intermolecular interactions has a direct influence on the self-assembly of polymer systems. Furthermore, we demonstrate that the Lewis-adduct driven self-assembly in the poly(2-(dimethylamino)ethyl methacrylate)-polystyrene (PDMAEMA-PS) diblock copolymer system in toluene leads to the formation of nanoscale spherical micelles, vesicles, and large compound vesicles when the PDMAEMA block mole fraction increases relative to the PS block. The work presented here emphasizes that non-covalent, intermolecular interactions will result in a bond polarization event that then leads to larger length scale changes (i.e., nanoscale self-assembly). We envision that analogous bond polarization effects occur in many non-covalent intermolecular interactions and is the underlying reason for many supramolecular self-assembly processes.

2. Results and Discussion

Previously, we demonstrated that the formation of Lewis adducts in polymer systems induces a phase change, which was termed as a reaction-induced phase transition (RIPT).[24] The non-covalent bond between BCF and the PDPPS block drives the self-assembly of the diblock copolymer into micelles, then higher order structures, following a two-step process.[25] Here, we have explored a different polymer from PDPPS (i.e., PDMAEMA) as the polyLB block to determine how the chemical functionality of the Lewis base influences the self-assembly and to remove potential arene-perflouroarene interactions[26,27] between the aromatic rings of PDPPS and fluorine atoms of BCF. Hence, switching from an aromatic to an aliphatic polyLB system was crucial to validate the Lewis adduct-induced self-assembly, while eliminating the possibility of other potential non-covalent interactions.

2.1 Synthesis of diblock copolymers

PDMAEMA-PS diblock copolymers were synthesized using sequential reversible addition-fragmentation chain transfer (RAFT) polymerization to control block composition, molecular weight, and mole fraction (**Figure 1a**). The PDMAEMA block was synthesized first and exhibited a number-average molecular weight (M_n = 10.9 kg/mol) and a dispersity ($Đ$ = 1.12). PDMAEMA was then utilized as a macro-CTA to polymerize styrene, yielding six PDMAEMA-PS diblock copolymers with constant PDMAEMA molecular weight and increasing PS molecular weight. Synthesis procedures are detailed in the Experimental Section (Supporting Information).

Upon chain extension of the PS block from the PDMAEMA block, additional ^{1}H NMR signals at 6.5-7.5 ppm are detected from the styrene aromatic protons. Using ^{1}H NMR data, the signal intensity of two methylene protons of the PDMAEMA at 4.1 ppm was compared to five

aromatic protons of the PS at 6.5-7.5 ppm, to estimate the mole fraction of the PDMAEMA block as 0.12, 0.3, 0.46, 0.5, 0.64 and 0.83 for PDMAEMA, as shown in **Figure 1b**. The molar compositions of the $PDMAEMA_x$-PS_y diblock copolymer, where x and y designate the mole ratio of the PDMAEMA and PS blocks, respectively, are shown in **Figure 1b**. The molecular weights of the diblock copolymers obtained from size-exclusion chromatography (SEC) using DMF/LiBr as the mobile phase is reported in **Table 1**.

A multi-angle light scattering detector attached to the SEC was used to measure the absolute M_n for all diblock copolymers. Therefore, dn/dc values for each diblock copolymer composition were calculated using ^{1}H NMR mole fractions. The SEC plot in **Figure 1c** indicates that the M_n of the diblock copolymer increases from 13.5 kg/mol to 69.7 kg/mol, demonstrating a significant increase in molecular weight with the elongation of the PS chain length. The six different diblock copolymers reported here are labeled as PDMAEMAX-PSY, where X and Y are the molecular weights of the respective blocks. The composition and molecular parameters of the six polymers synthesized are listed in **Table 1**.

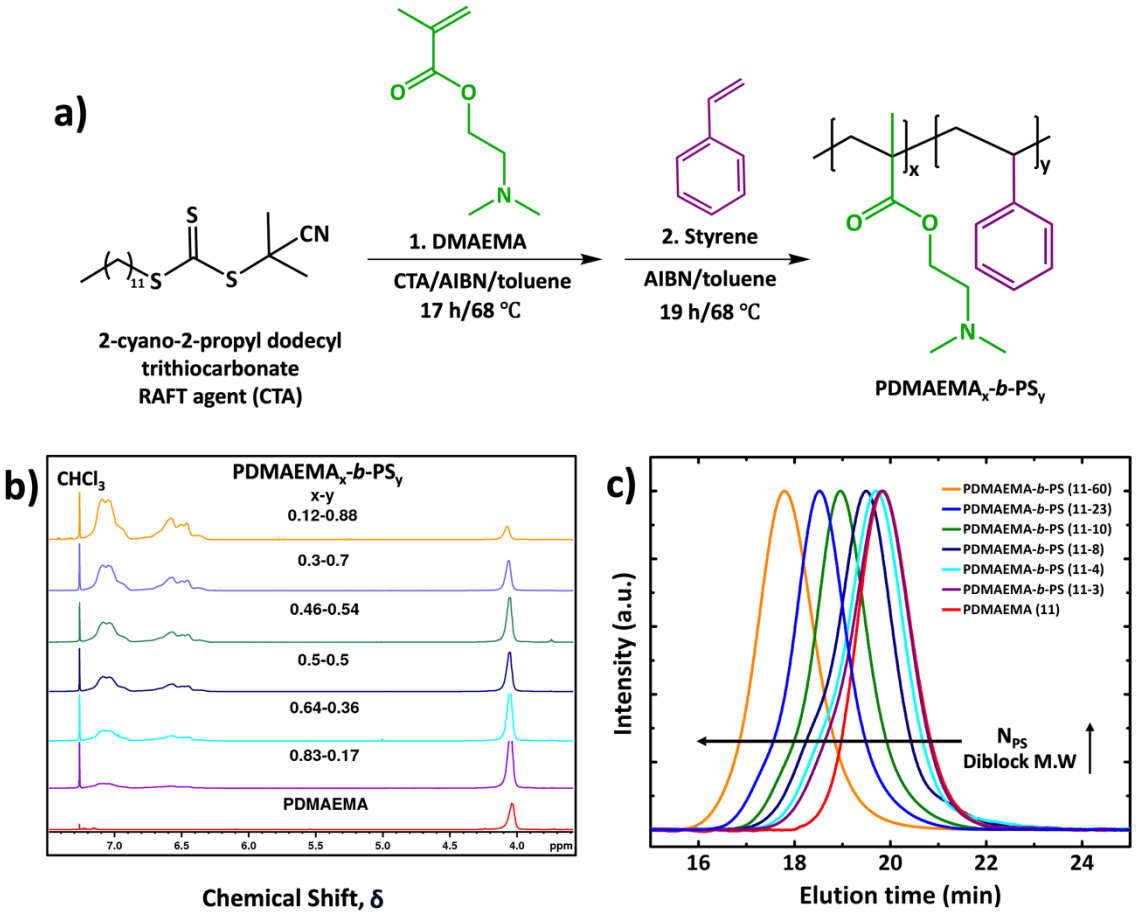

Figure 1. Synthesis and molecular weight characterization of PDMAEMA-*b*-PS diblock copolymers. a) Sequential RAFT polymerization of diblock copolymers. First, the DMAEMA is polymerized, which is then chain-extended with PS to control the composition of the two blocks. b) Stacked ^{1}H NMR spectra in $CDCl_3$ recorded for a series of PDMAEMA$_x$-*b*-PS$_y$ diblock copolymers, where x and y represents the mole ratio of the corresponding block. c) Normalized SEC traces, where DMF with 0.05 M LiBr salt is the mobile phase, mark a significant increase in the diblock molecular weight (red – homopolymer PDMAEMA precursor; elution time decreases from right to left (i.e., purple to orange – signifying an increase in copolymer molecular weight).

Table 1. Molecular characteristics of PDMAEMA-PS diblock copolymers

Diblock Copolymers[a]	Molar Composition[b]	$M_{n,diblock}$ (kg/mol)	$Đ$[c]	$M_{n,PS}$ (kg/mol)[d]
PDMAEM11-PS60	12/88	69.7	1.14	58.8
PDMAEM11-PS23	30/70	33.6	1.12	22.7
PDMAEM11-PS10	46/54	21.3	1.16	10.4
PDMAEM11-PS8	50/50	19.2	1.19	8.3
PDMAEM11-PS4	64/36	15.2	1.17	4.3
PDMAEM11-PS3	83/17	13.5	1.16	2.6

[a] Diblock copolymers (PDMAEMA-PS) synthesized via sequential RAFT polymerization using macro-CTA PDMAEMA of M_n = 10.9 kg/mol and $Đ$ = 1.12. The values after the polymer block abbreviation represent the block molecular weight in kg/mol.

[b] Copolymer composition (PDMAEMA/PS) determined from ^{1}H NMR in $CDCl_3$ by comparing the PS aromatic 5H signal integration to the PDMAEMA 2H signal.

[c] Number average molecular weight (M_n) and dispersity ($Đ$) determined using SEC in DMF with 0.05 M LiBr

[d] M_n of PS block in each composition obtained by subtracting $M_{n,PDMAEMA}$ from $M_{n,diblock}$

2.2 Nanoscale self-assembly

The colloidal nanostructures formed from the Lewis adduct-induced self-assembly of BCF/PDMAEMA-PS mixtures in toluene was examined by maintaining boron to nitrogen molar ratio as 1 (i.e., B/N = 1.0). **Figure 2** illustrates the self-assembly process where a 1 mL BCF solution in dry toluene was added dropwise at the rate of 1 drop/ 30 s to the 1 mL of diblock copolymer solution under vigorous stirring. The concentrations of the diblock and BCF solutions are detailed in **Table S1**. The addition of BCF to PDMAEMA-PS induced self-

assembly similarly to the previously published PDPPS-PS system.[25] All resulting solutions were colloidally stable, and the structure of the nanoscale structures was characterized using transmission electron microscopy (TEM), dynamic light scattering (DLS), and small-angle X-ray scattering (SAXS).

The formation of the Lewis adduct that is attached to the polymer was previously predicted to lead to a demixing process due to the favorable interactions. The self-assembled nanoscale structures are expected to adopt a core-corona morphology, where the solvent-miscible block forms the corona and the incompatible block forms the core.[28,29] Here, the self-assembled colloidal structures are expected to exhibit a core containing the BCF/PDMAEMA adduct, and the solvent-compatible PS block swollen in toluene as the corona (**Figure 2**).

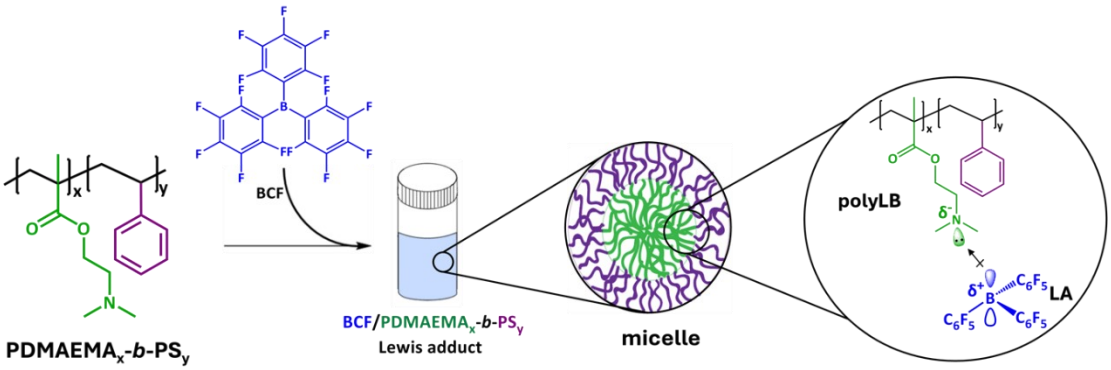

Figure 2. Self-assembly procedure to prepare colloidal nanostructures driven by the formation of Lewis adducts. Dropwise addition of BCF into a solution containing PDMAEMA-PS triggers self-assembly that is induced by the formation of non-covalent bonds. Spherical micelles and vesicles form using different PDMAEMA-PS block mole fractions at B/N molar ratio 1.0. The colloidal nanostructures adopt a core-corona morphology, where the toluene compatible neutral block PS forms the corona and the BCF/PDMAEMA Lewis adduct appears as a core of the micelle.

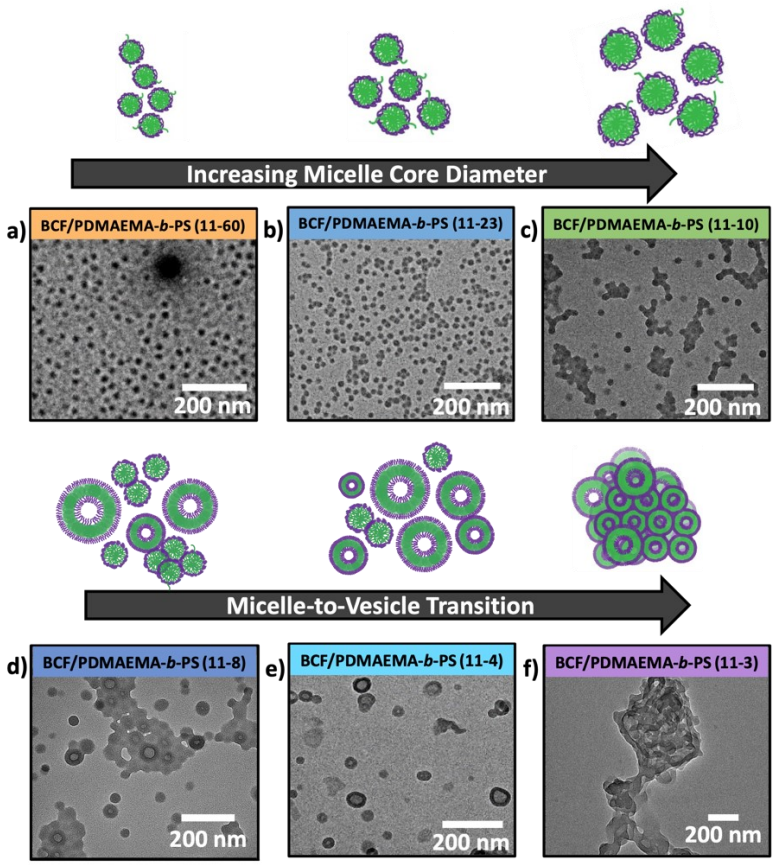

Figure 3. TEM analysis of self-assembled nanostructures formed using Lewis-adduct induced phase-transitions. a-f) Representative TEM images of self-assembled nanostructures of PDMAEMA-PS mixed with BCF at a B/N = 1.0 in toluene. Spherical micelles, vesicles, and large compound vesicles form with increasing PDMAEMA mole fraction (i.e., decreasing PS molecular weight). a-c) The core diameter of the spherical micelles increases from 16 to 25 nm for samples PDMAEMA11-PS60, PDMAEMA11-PS23, and PDMAEMA11-PS10. d-f) The presence of vesicles are seen for samples PDMAEMA11-PS8 and PDMAEMA11-PS4, and large compound vesicles form for PDMAEMA11-PS3.

TEM was employed to visualize the morphology of the self-assembled nanostructures prepared using PDMAEMA-PS with different block molecular weights (**Figure 3**). The TEM images clearly show a transition in nanoscale morphologies with decreasing PS molecular weight. Initially, at high PS molecular weights (60, 23, and 10 kg/mol in **Figures 3a-c**), the

copolymer forms well-defined spherical micelles. The particle size distribution graphs in **Figure S8** show that the core diameter of these micelles progressively increases, measuring 16 ± 3 nm, 18 ± 4 nm, and 26 ± 4 nm for PS molecular weights 60, 23, and 10 kg/mol, respectively. The increase in micelle diameter suggests a direct correlation of increasing core size with PS molecular weight.

A notable morphological transition is observed as the PS molecular weight is decreased further to 8 kg/mol (**Figure 3d**), where both sphere and vesicle structures coexist, indicating the onset of a morphology transformation. The presence of spherical micelles and vesicles are seen for samples PDMAEMA11-PS8 and PDMAEMA11-PS4 (**Figures 3d, 3e**), but the number ratio of micelles-to-vesicles decreases with decreasing PS molecular weight. As seen in **Figure 3**, the micelle-to-vesicle transition is not abrupt, but gradual where the micelle-to-vesicle number ratio decreases going from 1.6:1 for PDMAEMA11-PS8 to 1:3.7 for PDMAEMA11-PS4. Over 450 micelles and vesicles were counted for each sample. Due to phase coexistence, SAXS profiles were difficult to fit (see **Figure S15**). Finally, at the lowest PS molecular weight (PDMAEMA11-PS3, **Figure 3f**), large compound vesicles[30] (61 ± 15 nm) are evident, which are complex vesicle aggregates.

The reported nanostructured morphologies of spherical micelles, vesicles, and large compound vesicles shown in **Figure 3** follow a similar trend to amphiphilic diblock copolymer systems with increasing hydrophobic block content. Here, instead of tuning the hydrophobic block content, the mole fraction of the polyLB is changed. The PDMAEMA block molecular weight is constant for all samples and the PS block length is varied, resulting in a change of the polyLB mole fraction. When the degree of polymerization of the PS corona chain (N_{PS}) is very long compared to the PDMAEMA block, the polymer micelles are preferred due to the corona block chains.[31,32] The long PS chains provide a strong steric barrier that prevents the BCF/PDMAEMA adduct cores from coming into direct contact with each other, favoring the

formation of the most stable morphology (i.e., spheres, as seen in **Figure 3a-c**). Decreasing N_{PS} from 770 to 125, where $N_{PDMAEMA}$ = 69, results in larger micelles. A further decrease in N_{PS} to 105 leads to a micelle and vesicle phase co-existence (**Figure 3d, e**).[33] Finally, when N_{PS} = 25, only large compound vesicles are present in the system (**Figure f**). Therefore, the corona chain length is a critical factor in controlling the resulting nanoscale morphologies when the PolyLB block length is constant. Supporting Information includes additional TEM images (**Figure S9-S14**) for all the compositions showing nanostructures at lower to higher magnification.

Although the morphology transition shown in **Figure 3** is similar to traditional amphiphilic diblock copolymer systems, there are clear differences. First, the spherical micelle and vesicle phase co-existence window is large. None of the PDMAEMA-PS block copolymers results in a sample with only vesicles when B/N = 1.0 . Second, interestingly, no worm-like micelles form. One possible reason for not seeing worm-like micelles is that the composition window for worm-like micelles is narrow. Finally, the formation of large compound vesicles, which was first reported by Eisenberg and co-workers, typically occurs at elevated salt concentrations for poly(styrene)-poly(acrylic acid) (PS-PAA). The Lewis adduct-induced self-assembly reported here is in toluene and therefore no salt is present. The discrepancies in self-assembled morphologies reported here as compared to traditional amphiphilic block copolymers could be due to fundamental differences in the self-assembly mechanism, which is currently being investigated.

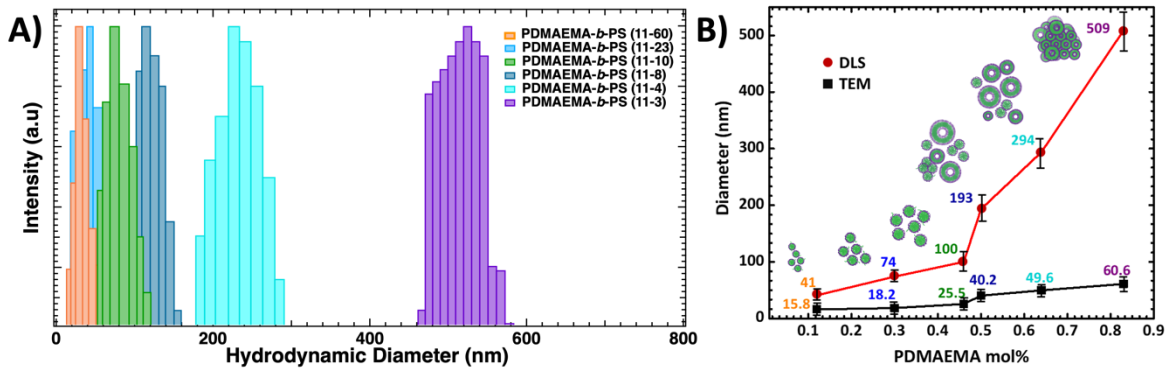

Figure 4. DLS and TEM comparison of colloidal nanostructure dimensions. a) All six PDMAEMA-PS samples at a B/N = 1.0 in toluene were analyzed using DLS. The DLS plot exhibits an increase in particle size with decreasing PS molecular weight. b) A plot showing the size differences of the colloidal structures from DLS and TEM techniques. Size ranges ~ 40-500 nm (DLS) and ~16-60 nm (TEM). DLS measures the hydrodynamic diameter of the particles and therefore we see larger size in comparison to TEM.

The colloidal nanostructures were further investigated using DLS. The PDMAEMA-PS diblock copolymer nanostructures at a B/N = 1.0 in toluene exhibit a monomodal particle size distribution, with mean hydrodynamic diameters (d_H) ranging from 40 to 500 nm (**Figure 4a**). The red line in **Figure 4b** represents d_H for the six different PDMAEMA-PS diblock copolymer samples obtained from DLS, while the black trace indicates the TEM results. Interestingly, the increase in the d_H of the colloidal nanostructures with respect to PDMAEMA block mole fraction (**Figure 4b**) is significantly greater than the core dimension increase assessed from TEM (**Figure 3**). The size differences observed between DLS and TEM are expected, as DLS accounts for both the core and corona chains in the solvated state, while TEM focuses solely on the core dimensions. As a result, the nanoscale measurements from DLS are consistently larger than those from TEM, which aligns with the presence of spherical micelles in the samples. For the samples containing vesicles, the size distribution is much broader, leading to increased light scattering from larger vesicles, resulting in an overall larger

hydrodynamic diameter. There is a potential of vesicle aggregates that would increase the hydrodynamic diameter, but the solutions are colloidally stable and are therefore not expected to be the reason for the larger size measured from DLS as compared to TEM. Additional SAXS measurements were performed to provide insight into the nanoscale domains and are consistent with the TEM data, as detailed in section S4 and **Figure S15** in the Supporting Information.

2.3 Binding constant and dielectric constant measurements

As discussed in the previous section, BCF addition leads to self-assembly in polyLB based diblock copolymers, yet the connection between molecular-level transitions during non-covalent binding and larger-scale organization remains elusive. To elucidate the self-assembly mechanism, first ^{1}H NMR spectroscopic titrations were employed to confirm that the adduct did form and to calculate equilibrium constants.[34,35] All titration experiments were conducted in a glove box under an argon atmosphere to maintain a dry environment. A series of samples with constant DMAEMA monomer concentrations and increasing BCF concentrations in tol-d_8 (**Figure 5a**) were prepared and analyzed using ^{1}H NMR spectroscopy. The concentrations are reported in the **Table S2**. The chemical shifts were determined using the spectra plotted in **Figure 5b** for different B/N ratios ranging from 0.2 to 1. Each spectrum shows the chemical shift for protons 'a' (O–C**H**$_2$) and 'b' (N–C**H**$_2$). In this system, the nitrogen atom in DMAEMA (a Lewis base) donates electron density to the boron atom in BCF (a Lewis acid), leading to increased shielding and resulting in upfield shifts in the NMR spectra. The observed upfield shifts for both protons a (4.15 to 3.51 ppm) and b (2.30 to 1.76), suggest that the electron density around these atoms increases as the B/N ratio increases, due to the formation of a stronger Lewis acid-base adduct with higher BCF content. A binding isotherm was obtained by plotting the magnitude of variation in chemical shift, $\Delta\delta$, associated with a resonance

assigned to DMAEMA against the BCF concentration (**Figure 5c**). This isotherm was subsequently analyzed using a 1:1 binding model.[25,35,36]

$$\Delta_{obs} = \Delta_{max} \frac{(K_d+[LA]_0+[LB]_0)-\sqrt{(K_d+[LA]_0+[LB]_0)^2-4([LA]_0[LB]_0)}}{2[LB]_0} \quad \textbf{(Eq. 1)}$$

Using the above expression (**Eq. 1**), the binding isotherms in **Figure 5c** were fitted to a non-linear regression analysis and the K_d values for BCF/DMAEMA complex were obtained as 1.4 × 10^{-2} M and 3.5 × 10^{-2} M using the proton a and b, respectively.

Additionally, ^{19}F NMR spectra in **Figure S15** show three distinct signals, referred as 1, with a ratio of 2:1:2 corresponding to the *ortho* (-134.95 ppm), *para* (-155.85 ppm), and *meta* (-163.32 ppm) fluorine atoms of BCF. A significant upfield shift, highlighted in red in the same figure, is observed due to the 1:1 adduct formation between BCF and DMAEMA. The particular large shift (Δδ = 3.45 ppm) of the *para* fluorine atoms is indicative of the transition from a tri-coordinated to a tetra-coordinated boron.[37]

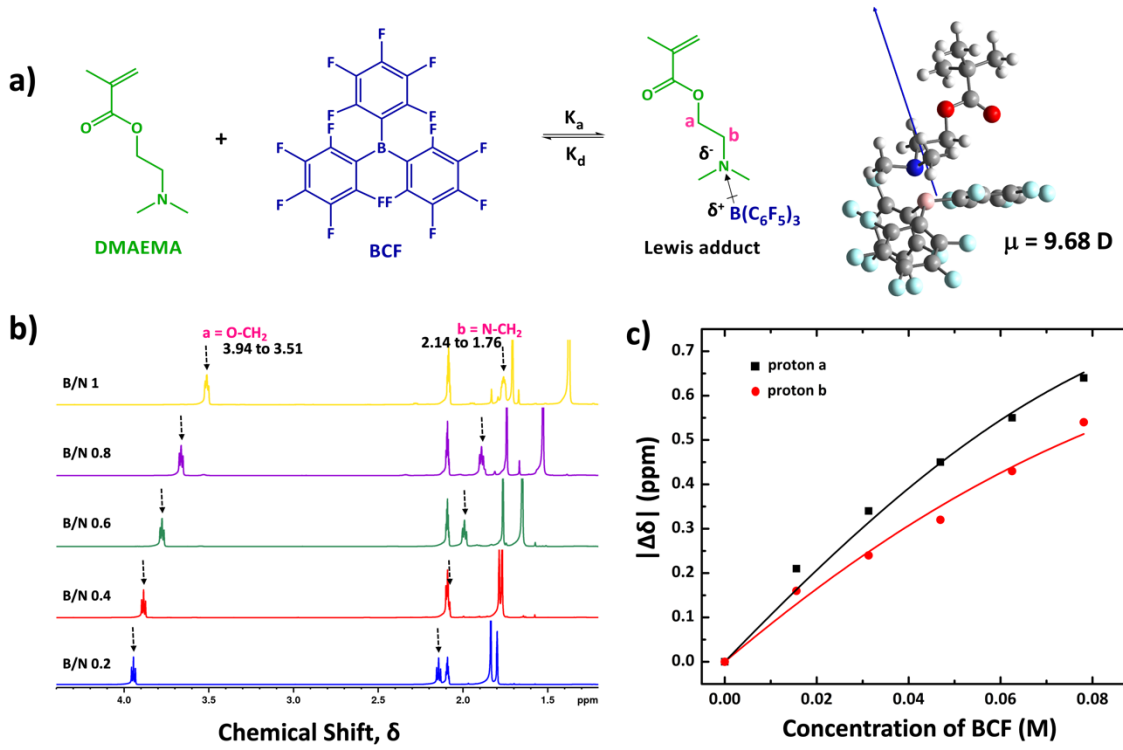

Figure 5. Determination of K_d using NMR titrations and static dielectric constant measurements using DRS. a) Schematic representation of the reaction between Lewis base DMAEMA and Lewis acid BCF, leads to the formation of a Lewis adduct. Right most image displays the dipole moment (μ = 9.68 D) of the adduct as obtained from the DFT simulation calculation. b) Stacked ^{1}H NMR spectra for BCF/DMAEMA adducts in tol-d_8 varying B/N mole ratio from 0.2 to 1.0 to record the change in chemical shift in ppm for proton a and b. c) Binding isotherms for the titration of BCF to DMAEMA, where symbols signify the experimental data and the lines represent the fits using a 1:1 binding model.

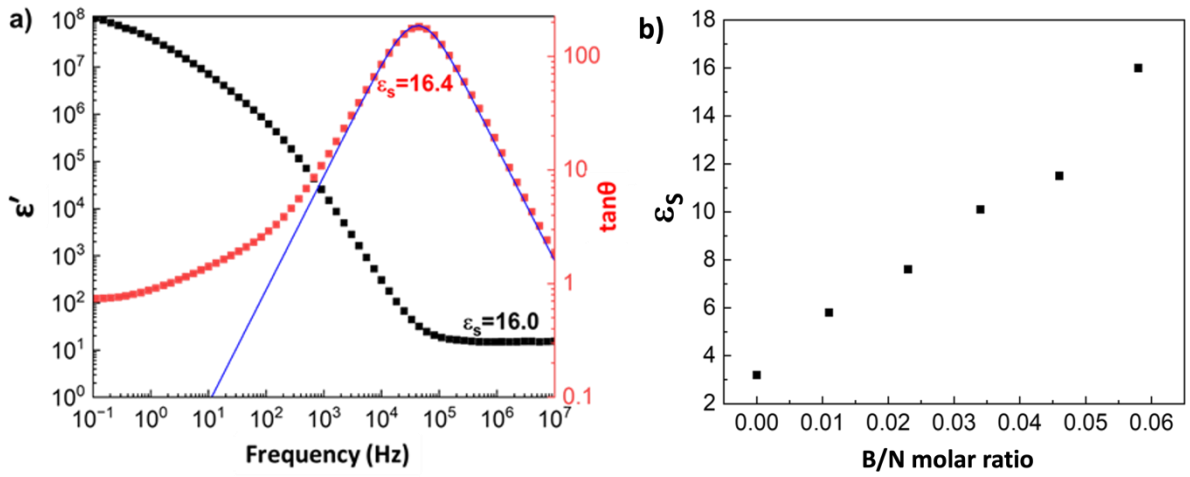

Figure 6. Determination of static dielectric constant measurements using DRS. a) Permittivity (black squares) and loss tangent (red squares) spectra for sample B/N = 0.058. The static dielectric constant was obtained both through the flat level of the permittivity (black squares) in the MHz range and by fitting the dielectric loss tangent (red squares) to **Eq. 2** (red line) and calculating using **Eq. 3**. b) Static dielectric constant of BCF and DMAEMA mixtures at 25 °C at various B/N molar ratios.

The static dielectric (ε_s) constant of BCF/DMAEMA mixtures was measured by dielectric relaxation spectroscopy (DRS), detailed in the Experimental Section (Supporting Information). As shown in **Figure 6a**, the static dielectric constant of adduct at B/N = 0.058 was obtained using two separate methods. In the first method, the static dielectric constant is obtained from the flat level of the permittivity (black squares in **Figure 6a**) in the MHz range. For the second method, the static dielectric constant was obtained by fitting the dielectric loss tangent (red squares in the same figure) to the Debye equation:

$$\tan\theta = \frac{\omega\tau}{1+\omega^2\tau^2/M} \qquad \textbf{(Eq. 2)}$$

where, τ is the relaxation time of the electrode polarization process, and M is the ratio of the sample thickness to twice the Debye length. Both τ and M are used as fitting parameters from **Eq. 2**, to obtain ε_s using the following equation: [38]

$$\varepsilon_S = \frac{\tau \sigma_{DC}}{\varepsilon_0 M} \quad \textbf{(Eq. 3)}$$

where, σ_{DC} is the DC-conductivity obtained from the plateau on the conductivity spectrum and ε_0 is the permittivity of vacuum. Graphs corresponding to other B/N ratios are included in **Figure S16(a-f)**. As shown in **Figure 6a** and **Figure S16(a-f)**, the static dielectric constant obtained from these two methods is quite similar, thus validating the static dielectric constant values. The static dielectric constant of adducts vs B/N ratio is plotted in **Figure 6b**. It is apparent that the static dielectric constant increases sharply with an increase in the B/N ratio, thus qualitatively proving the static dielectric constant of the adduct is much larger than that of DMAEMA ($\varepsilon_{s,adduct} >> \varepsilon_{s,DMAEMA}$).

By assuming that the overall measured static dielectric constant of the mixtures follows the simple additivity of the static dielectric constant from DMAEMA, BCF/DMAEMA adduct, and left-over BCF (commonly used in dilute solutions),[39] the static dielectric constant contribution of BCF/DMAEMA adduct ($\varepsilon_{s,\ adduct}$) at each B/N ratio can be calculated using the following equation:

$$\varepsilon_{s,adduct} = \varepsilon_{s,mixture} - \omega_{DMAEMA}\varepsilon_{s,DMAEMA} - \omega_{BCF}\varepsilon_{s,BCF} \quad \textbf{(Eq. 4)}$$

where, ω_{DMAEMA} represents the molar ratio of left-over DMAEMA in the mixture (**Table S4**), $\varepsilon_{s,DMAEMA}$ = 3.2 represents the static dielectric constant of DMAEMA measured using DRS, ω_{BCF} represents the molar ratio of left-over BCF in the mixture (**Table S4**), $\varepsilon_{s,BCF}$ = 2.3 represents the static dielectric constant of BCF (calculated by the Onsager equation (**Eq. 5**), with the dipole moment of BCF = 0.92 D as obtained from DFT simulation, **Figure S16g**). Also, the dipole moment of DMAEMA approximated from DFT simulation is 2.23 D as shown

in **Figure S16h**. The dipole moment of BCF/DMAEMA adduct was then calculated using Onsager equation:[40]

$$\frac{p_0 m^2}{9\varepsilon_0 kT} = \frac{(\varepsilon_S - \varepsilon_\infty)(2\varepsilon_S + \varepsilon_\infty)}{\varepsilon_S(\varepsilon_\infty + 2)^2} \quad \textbf{(Eq. 5)}$$

where, p_0 is the dipole moment density, m is the dipole moment, ε_0 is the vacuum permittivity, k is the Boltzmann constant, and $\varepsilon_\infty = 2$ is the high-frequency dielectric constant due to electronic polarization. The dipole moment of BCF/DMAEMA adduct calculated at each B/N ratio, represented in **Table 2**, shows that it remains closer to constant (~ 12.5 D) at different B/N ratios. Additionally, these values agree roughly with the dipole moment obtained from the DFT simulation (9.68 D, right most image in **Figure 6a**). These DFT results support the validity of DRS experiments to calculate the dipole moment of the adduct.

Table 2. Adduct dipole moment calculated for each B/N ratio mixture using Eq. 4 and Eq. 5

BCF/DMAEMA (B/N molar ratio)	**m_{adduct} (D)**
0.011	12.0
0.023	11.3
0.034	12.8
0.046	12.4
0.058	13.9

The dipole moment of the Lewis adduct here formed by a dative bond is larger than that in typical covalent molecules, where electronegativity differences drive dipoles, and also larger than previously measured values for Lewis adducts in the gas phase.[41,42] The reason for the difference between the dipole reported here as compared to gas-phase measurements is that the gas-phase measurements involved smaller molecules with shorter distances between

interacting atoms. In this system, the electron density is more widely distributed over the adduct, increasing the distance between donor-acceptor bonding charges and leading to a higher dipole moment.[43] Thus, by utilizing dynamic chemical bonding during Lewis adduct formation, we have designed polymeric adduct mixtures that exhibit significantly large dipoles through non-covalent interactions.

Dipole-directed assembly is critical in synthetic and biological macromolecular systems such as polyzwitterions, polyelectrolytes, coacervation, and proteins.[44] The role of dipole-dipole interactions results in intermolecular associations that lead to a variety of aggregate structures. Notably many of these structures cannot be predicted by orientationally-averaged (isotropic) interaction potentials,[45,46] such as the Lennard-Jones potential or the Flory contact repulsion, both of which are ubiquitous in modelling polymer self-assembly. While theory predicts that mismatched polarity between monomers leads to an increase in the effective Flory interaction,[47,48] the combination of reversible association alongside changes in polarity remains comparatively unexplored.

3. Conclusions

Here, we present a comprehensive analysis of the self-assembly behavior of diblock copolymers induced by non-covalent interactions, specifically focusing on Lewis adduct binding-induced bond polarization. We demonstrate that introducing a small molecule, BCF, as a Lewis acid to an aliphatic diblock copolymer system containing PDMAEMA as a polymerized Lewis base, polyLB, triggers self-assembly, leading to the formation of different nanostructured colloidal aggregates that depend on the polyLB block mole fraction. These nanoscale structures adopt a core-corona morphology, where the solvent-incompatible BCF/PDMAEMA adduct forms the core, and the solvent miscible PS block forms the corona. Increasing the PDMAEMA block mole fraction first increases the size of the spherical micelles

and for large PDMAEMA creates a micelle-to-vesicles transition, and ultimately to complex large compound vesicles, thus highlighting the critical role of the block copolymer composition in dictating the final morphology of the self-assembled structures.

The key finding of this study is the role of bond polarization during Lewis adduct formation in driving the self-assembly process, which is supported by the dielectric constant measurements of the BCF/DMAEMA adduct mixtures. The concept of binding-induced bond polarization offers a new perspective on how non-covalent interactions can be utilized to control the self-assembly of polymers. By revealing the connection between bond polarization and self-assembly, this study provides a framework for exploring other non-covalent interactions and their potential to drive the formation of complex nanostructures. Future research could expand on these findings by investigating different polymer systems, varying the types of Lewis acids and bases used, and exploring the effects of other external stimuli on the self-assembly process, promising a new kind of smart, responsive materials designed for various biomedical and catalysis applications.

Data Availability

The raw data files for this article are available at Data Commons at Penn State at https://doi.org/10.26208/NRKB-VW46.

Acknowledgements

This research was supported by the National Science Foundation under grant CHE MSN 2203675 and 2203905. X-ray scattering experiments were conducted at the National Synchrotron Light Source II (NSLS II) facility at CMS 11-BM, located at Brookhaven National Laboratory (BNL). NSLS II is a user facility operated by the Office of Science of the U.S.

Department of Energy. The authors gratefully acknowledge Dr. Ruipeng Li at BNL for his assistance with the X-ray scattering experiments at the beamline.

Author information

Authors and Affiliations

Department of Materials Science and Engineering at the Pennsylvania State University, University Park, PA, USA

Shubhra Goel, Zitan Huang, Ralph H. Colby, Robert J. Hickey

Materials Research Institute at the Pennsylvania State University, University Park, PA, USA

Ralph H. Colby, Robert J. Hickey

Department of Chemical and Biomolecular Engineering at the University of Pennsylvania, Philadelphia, PA, USA

Robert A. Riggleman

Contributions

S.G. and R.J.H. conceptualized and designed the research. S.G synthesized, prepared, and characterized the self-assembled nanostructures. Z.H. conducted the dielectric measurements and analyzed the data, under the supervision of R.H.C. R.A.R. performed and produced the computational results. R.J.H. supervised the entire research. All authors contributed to the writing, discussion and the data analysis.

Corresponding author

Correspondence to Robert J. Hickey, rjh64@psu.edu.

Ethics declarations

Competing Interests

The authors declare no competing interests.

Supplementary information

The supplementary data file includes the Experimental Section, detailing the materials and characterization techniques used. The synthesis of the homopolymer (PDMAEMA) and all diblock copolymers (PDMAEMA$_x$-*b*-PS$_y$) is described in sections S2.1 to S2.2.6, followed by the general procedure for preparing BCF/PDMAEMA$_x$-*b*-PS$_y$ Lewis adducts. Nanoscale self-assembly using SAXS analysis is discussed in the subsequent section. The supporting figures in the file include labelled ^{1}H NMR spectra of all polymers, SAXS patterns (both experimental and model fit), and dielectric plots (permittivity and dielectric loss). Additionally, sample preparation details and findings from the respective characterization techniques are provided in the supporting tables.

References

(1) Brunsveld, L.; Folmer, B. J. B.; Meijer, E. W.; Sijbesma, R. P. Supramolecular Polymers. *Chem Rev* **2001**, *101* (12), 4071–4097. https://doi.org/10.1021/cr990125q.

(2) Yolsal, U.; Horton, T. A. R.; Wang, M.; Shaver, M. P. Polymer-Supported Lewis Acids and Bases: Synthesis and Applications. *Prog Polym Sci* **2020**, *111*, 101313. https://doi.org/10.1016/j.progpolymsci.2020.101313.

(3) Lundberg, D. J.; Brown, C. M.; Bobylev, E. O.; Oldenhuis, N. J.; Alfaraj, Y. S.; Zhao, J.; Kevlishvili, I.; Kulik, H. J.; Johnson, J. A. Nested Non-Covalent Interactions Expand the Functions of Supramolecular Polymer Networks. *Nat Commun* **2024**, *15* (1). https://doi.org/10.1038/s41467-024-47666-x.

(4) Crippa, M.; Perego, C.; de Marco, A. L.; Pavan, G. M. Molecular Communications in Complex Systems of Dynamic Supramolecular Polymers. *Nat Commun* **2022**, *13* (1). https://doi.org/10.1038/s41467-022-29804-5.

(5) Samanta, S.; Raval, P.; Manjunatha Reddy, G. N.; Chaudhuri, D. Cooperative Self-Assembly Driven by Multiple Noncovalent Interactions: Investigating Molecular Origin and Reassessing Characterization. *ACS Cent Sci* **2021**, *7* (8), 1391–1399. https://doi.org/10.1021/acscentsci.1c00604.

(6) Guo, J.; Tian, C.; Xu, B. Biomaterials Based on Noncovalent Interactions of Small Molecules. *EXCLI J* **2020**, *19*, 1124–1140. https://doi.org/10.17179/excli2020-2656.

(7) Syamala, P. P. N.; Würthner, F. Modulation of the Self-Assembly of π-Amphiphiles in Water from Enthalpy- to Entropy-Driven by Enwrapping Substituents. *Chemistry - A European Journal* **2020**, *26* (38), 8426–8434. https://doi.org/10.1002/chem.202000995.

(8) Aida, T.; Meijer, E. W.; Stupp, S. I. Functional Supramolecular Polymers. *Science (1979)* **2012**, *335*. https://doi.org/10.1126/science.1205962.

(9) Zhu, Y.; Liu, L.; Du, J. Probing into Homopolymer Self-Assembly: How Does Hydrogen Bonding Influence Morphology? *Macromolecules* **2013**, *46* (1), 194–203. https://doi.org/10.1021/ma302176a.

(10) Yoshida, E.; Kunugi, S. Micelle Formation of Nonamphiphilic Diblock Copolymers through Noncovalent Bond Cross-Linking. *Macromolecules* **2002**, *35* (17), 6665–6669. https://doi.org/10.1021/ma020275u.

(11) Folmer, B. J. B.; Sijbesma, R. P.; Versteegen, R. M.; Van Der Rijt, J. A. J.; Meijer, E. W. Supramolecular Polymer Materials: Chain Extension of Telechelic Polymers Using a Reactive Hydrogen-Bonding Synthon. *Advanced Materials* **2000**, *12* (12), 874–878. https://doi.org/10.1002/1521-4095(200006)12:12<874::AID-ADMA874>3.0.CO;2-C.

(12) Yang, D.; Gao, S.; Fang, Y.; Lin, X.; Jin, X.; Wang, X.; Ke, L.; Shi, K. The π-π Stacking-Guided Supramolecular Self-Assembly of Nanomedicine for Effective Delivery of Antineoplastic Therapies. *Nanomedicine* **2018**, *13* (24), 3159–3177. https://doi.org/10.2217/nnm-2018-0288.

(13) Lai, Y.; Lei, Y.; Xu, X.; Li, Y.; He, B.; Gu, Z. Polymeric Micelles with π-π Conjugated Cinnamic Acid as Lipophilic Moieties for Doxorubicin Delivery. *J Mater Chem B* **2013**, *1* (34), 4289–4296. https://doi.org/10.1039/c3tb20392a.

(14) Stornaiuolo, M.; De Kloe, G. E.; Rucktooa, P.; Fish, A.; Van Elk, R.; Edink, E. S.; Bertrand, D.; Smit, A. B.; De Esch, I. J. P.; Sixma, T. K. Assembly of a π-π Stack of Ligands in the Binding Site of an Acetylcholine-Binding Protein. *Nat Commun* **2013**, *4* (May). https://doi.org/10.1038/ncomms2900.

(15) Sánchez-Iglesias, A.; Grzelczak, M.; Altantzis, T.; Goris, B.; Pérez-Juste, J.; Bals, S.; Van Tendeloo, G.; Donaldson, S. H.; Chmelka, B. F.; Israelachvili, J. N.; Liz-Marzán, L. M. Hydrophobic Interactions Modulate Self-Assembly of Nanoparticles. *ACS Nano* **2012**, *6* (12), 11059–11065. https://doi.org/10.1021/nn3047605.

(16) Faul, C. F. J. Ionic Self-Assembly for Functional Hierarchical Nanostructured Materials. *Acc Chem Res* **2014**, *47* (12), 3428–3438. https://doi.org/10.1021/ar500162a.

(17) Rest, C.; Kandanelli, R.; Fernández, G. Strategies to Create Hierarchical Self-Assembled Structures via Cooperative Non-Covalent Interactions. *Chem Soc Rev* **2015**, *44* (8), 2543–2572. https://doi.org/10.1039/c4cs00497c.

(18) Vermonden, T.; Van Steenbergen, M. J.; Besseling, N. A. M.; Marcelis, A. T. M.; Hennink, W. E.; Sudhölter, E. J. R.; Cohen Stuart, M. A. Linear Rheology of Water-Soluble Reversible Neodymium(III) Coordination Polymers. *J Am Chem Soc* **2004**, *126* (48), 15802–15808. https://doi.org/10.1021/ja0458928.

(19) Burnworth, M.; Tang, L.; Kumpfer, J. R.; Duncan, A. J.; Beyer, F. L.; Fiore, G. L.; Rowan, S. J.; Weder, C. Optically Healable Supramolecular Polymers. *Nature* **2011**, *472* (7343), 334–337. https://doi.org/10.1038/nature09963.

(20) Welch, G. C.; Bazan, G. C. Lewis Acid Adducts of Narrow Band Gap Conjugated Polymers. *J Am Chem Soc* **2011**, *133* (12), 4632–4644. https://doi.org/10.1021/ja110968m.

(21) Yolsal, U.; Horton, T. A. R.; Wang, M.; Shaver, M. P. Polymer-Supported Lewis Acids and Bases: Synthesis and Applications. *Prog Polym Sci* **2020**, *111*, 101313. https://doi.org/10.1016/j.progpolymsci.2020.101313.

(22) Yolsal, U.; Horton, T. A. R.; Wang, M.; Shaver, M. P. Cyclic Ether Triggers for Polymeric Frustrated Lewis Pair Gels. *J Am Chem Soc* **2021**, *143* (33), 12980–12984. https://doi.org/10.1021/jacs.1c06408.

(23) Vidal, F.; Gomezcoello, J.; Lalancette, R. A.; Jäkle, F. Lewis Pairs as Highly Tunable Dynamic Cross-Links in Transient Polymer Networks. *J Am Chem Soc* **2019**, *141* (40), 15963–15971. https://doi.org/10.1021/jacs.9b07452.

(24) Hickey, R. J. Controlling Polymer Material Structure during Reaction-Induced Phase Transitions. *Acc Mater Res* **2023**, *4* (9), 798–808. https://doi.org/10.1021/accountsmr.3c00071.

(25) Hilaire, T.; Xu, Y.; Mei, W.; Riggleman, R. A.; Hickey, R. J. Lewis Adduct-Induced Phase Transitions in Polymer/Solvent Mixtures. *ACS Polymers Au* **2022**, *2* (1), 35–41. https://doi.org/10.1021/acspolymersau.1c00024.

(26) Lee, G. Y.; Hu, E.; Rheingold, A. L.; Houk, K. N.; Sletten, E. M. Arene-Perfluoroarene Interactions in Solution. *Journal of Organic Chemistry* **2021**, *86* (12), 8425–8436. https://doi.org/10.1021/acs.joc.1c00921.

(27) Jacobsen, H.; Berke, H.; Döring, S.; Kehr, G.; Erker, G.; Fröhlich, R.; Meyer, O. Lewis Acid Properties of Tris(Pentafluorophenyl)Borane. Structure and Bonding in L-B(C6F5)3 Complexes. *Organometallics* **1999**, *18* (9), 1724–1734. https://doi.org/10.1021/om981033e.

(28) Howe, D. H.; Hart, J. L.; McDaniel, R. M.; Taheri, M. L.; Magenau, A. J. D. Functionalization-Induced Self-Assembly of Block Copolymers for Nanoparticle Synthesis. *ACS Macro Lett* **2018**, *7* (12), 1503–1508. https://doi.org/10.1021/acsmacrolett.8b00815.

(29) Lequieu, J.; Magenau, A. J. D. Reaction-Induced Phase Transitions with Block Copolymers in Solution and Bulk. *Polym Chem* **2021**, *12* (1), 12–28. https://doi.org/10.1039/d0py00722f.

(30) Zhang, L.; Eisenberg, A. Formation of Crew-Cut Aggregates of Various Morphologies from Amphiphilic Block Copolymers in Solution. *Polym Adv Technol* **1998**, *9*, 677–699. https://doi.org/10.1002/(SICI)1099-1581(1998100)9:10/11<677::AID-PAT845>3.0.CO;2-%23.

(31) Mai, Y.; Eisenberg, A. Self-Assembly of Block Copolymers. *Chem Soc Rev* **2012**, *41* (18), 5969–5985. https://doi.org/10.1039/c2cs35115c.

(32) Israelachvili, J. N.; Mitchell, D. J.; Ninham, B. W. Theory of Self-Assembly of Hydrocarbon Amphiphiles into Micelles and Bilayers. *Journal of the Chemical Society, Faraday Transactions 2: Molecular and Chemical Physics* **1976**, *72*, 1525–1568. https://doi.org/10.1039/F29767201525.

(33) Luo, L.; Eisenberg, A. Thermodynamic Size Control of Block Copolymer Vesicles in Solution. *Langmuir* **2001**, *17* (22), 6804–6811. https://doi.org/10.1021/la0104370.

(34) Thordarson, P. Determining Association Constants from Titration Experiments in Supramolecular Chemistry. *Chem Soc Rev* **2011**, *40* (3), 1305–1323. https://doi.org/10.1039/c0cs00062k.

(35) Mayer, R. J.; Hampel, N.; Ofial, A. R. Lewis Acidic Boranes, Lewis Bases, and Equilibrium Constants: A Reliable Scaffold for a Quantitative Lewis Acidity/Basicity Scale. *Chemistry - A European Journal* **2021**, *27* (12), 4070–4080. https://doi.org/10.1002/chem.202003916.

(36) Fielding, L. NMR Methods for the Determination of Protein-Ligand Dissociation Constants. *Curr Top Med Chem* **2003**, *3* (0), 39–53. https://doi.org/10.1002/9783527645947.ch5.

(37) Beringhelli, T.; Maggioni, D.; D'Alfonso, G. 1H and 19F NMR Investigation of the Reaction of B(C6F5)3 with Water in Toluene Solution. *Organometallics* **2001**, *20* (23), 4927–4938. https://doi.org/10.1021/om010610n.

(38) Klein, R. J.; Zhang, S.; Dou, S.; Jones, B. H.; Colby, R. H.; Runt, J. Modeling Electrode Polarization in Dielectric Spectroscopy: Ion Mobility and Mobile Ion Concentration of Single-Ion Polymer Electrolytes. *Journal of Chemical Physics* **2006**, *124* (14). https://doi.org/10.1063/1.2186638.

(39) Mei, W.; Rothenberger, A. J.; Bostwick, J. E.; Rinehart, J. M.; Hickey, R. J.; Colby, R. H. Zwitterions Raise the Dielectric Constant of Soft Materials. *Phys Rev Lett* **2021**, *127* (22), 228001. https://doi.org/10.1103/PhysRevLett.127.228001.

(40) Onsager, L. Electric Moments of Molecules in Liquids. *Journal of Americal Chemical Society* **1936**, *58* (8), 1486–1493. https://doi.org/10.1021/ja01299a050.

(41) Fiacco, D. L.; Mo, Y.; Hunt, S. W.; Ott, M. E.; Roberts, A.; Leopold, K. R. Dipole Moments of Partially Bound Lewis Acid - Base Adducts. *Journal of Physical Chemistry A* **2001**, *105* (2), 484–493. https://doi.org/10.1021/jp0031810.

(42) Hunt, S. W.; Fiacco, D. L.; Craddock, M.; Leopold, K. R. Correlation of Dative Bond Length and Donor Proton Affinity in Adducts of SO_3: A Good Predictor for HCCCN-SO_3. *J Mol Spectrosc* **2002**, *212* (2), 213–218. https://doi.org/10.1006/jmsp.2002.8554.

(43) Laubengayer, A. W.; Sears, D. S. Donor-Acceptor Bonding. III. Methyl Cyanide Addition Compounds of Boron Trichloride and Boron Trifluoride. *Journal of American Chemical Society* **1945**, *62*, 164–167. https://doi.org/10.1021/ja01218a004.

(44) Phillips, M.; Muthukumar, M.; Ghosh, K. Beyond Monopole Electrostatics in Regulating Conformations of Intrinsically Disordered Proteins. *PNAS nexus* **2024**, *3* (9), 367. https://doi.org/10.1093/pnasnexus/pgae367.

(45) Muthukumar, M. Dipole Theory of Polyzwitterion Microgels and Gels. *Gels* **2024**, *10* (6). https://doi.org/10.3390/gels10060393.

(46) Kumar, R.; Li, W.; Sumpter, B. G.; Muthukumar, M. Understanding the Effects of Dipolar Interactions on the Thermodynamics of Diblock Copolymer Melts. *Journal of Chemical Physics* **2019**, *151*, 054902. https://doi.org/10.1063/1.5114799.

(47) Martin, J. M.; Li, W.; Delaney, K. T.; Fredrickson, G. H. Statistical Field Theory Description of Inhomogeneous Polarizable Soft Matter. *Journal of Chemical Physics* **2016**, *145* (15). https://doi.org/10.1063/1.4964680.

(48) Israelachvili, J. N. *Intermolecular and Surface Forces*, III.; Netherlands, Elsevier Science, 2011, 1–674. https://doi.org/10.1016/C2009-0-21560-1.